Available online at www.sciencedirect.com

SciVerse ScienceDirect

Procedia Computer Science 9 (2012) 651 – 660

Procedia Computer Science

International Conference on Computational Science, ICCS 2012

# A Conditionally Stable Scheme for a Transient Flow of a Non-Newtonian Fluid Saturating a Porous Medium

M. F. El-Amin[a,b,*], Amgad Salama[a,c], and Shuyu Sun[a]

[a]*King Abdullah University of Science and Technology (KAUST), Thuwal 23955-6900, KSA*
[b]*Aswan Faculty of Science, South Valley University, Aswan 81528, Egypt*
[c]*Nuclear Research Center, AEA, Cairo, Egypt*

**Abstract**

The problem of thermal dispersion effects on unsteady free convection from an isothermal horizontal circular cylinder to a non-Newtonian fluid saturating a porous medium is examined numerically. The Darcy-Brinkman-Forchheimer model is employed to describe the flow field. The thermal diffusivity coefficient has been assumed to be the sum of the molecular diffusivity and the dynamic diffusivity due to mechanical dispersion. The simultaneous development of the momentum and thermal boundary layers are obtained by using finite difference method. The stability conditions are determined for each difference equation. Using an explicit finite difference scheme, solutions at each time-step have been found and then stepped forward in time until reaching steady state solution. Velocity and temperature profiles are shown graphically. It is found that as time approaches infinity, the values of friction factor and heat transfer coefficient approach the steady state values.

*Keywords:* Finite difference method; stability; non-Newtonian fluids; porous media; free convection

## 1. Introduction

A number of industrially important fluids such as foods, polymers, molten plastics, slurries and pulps display non-Newtonian fluid behavior. Non-Newtonian fluids exhibit a non-linear relationship between shear and strain rates. In most of the previous studies of non-Newtonian fluids flow through porous media, Darcy's law was used. For many practical applications, however, Darcy's law is not valid, and inertial effects may need to be taken into account. Several research works have been found in the literatures concerning the problem of coupled flow and heat transfer in saturated porous media including different set ups and boundary conditions. To highlight an incomplete list and for the sake of completion, we mention a number of these research work. Cheng [1] and Plumb [2] introduced a model for flow and heat transfer in porous media in which thermal dispersion effects are taken into consideration. Recently, Mansour and El-Amin [3] investigated the effects of thermal dispersion on non-Darcy axisymmetric free convection in a saturated porous medium with lateral mass transfer. On the other hand thermal dispersion-radiation effects on non-Darcy natural convection in a fluid saturated porous medium have been studied by Mohammadein and El-Amin [4]. Chen and Chen [5] presented similarity solutions for free convection on non-Newtonian fluids over vertical surfaces in porous media. Nakayama and Koyama [6] studied the natural convection

* Corresponding author. Tel.: +966-54-448-5177.
*E-mail address*: mohamed.elamin@kaust.edu.sa.


doi:10.1016/j.procs.2012.04.070

over a non-isothermal body of arbitrary shape embedded in a porous medium. Darcy-Forchheimer natural, forced and mixed convection heat transfer in power-law fluid saturated porous media was studied by Shenoy [7]. The problem of buoyancy induced flow of non-Newtonian fluids over a non-isothermal horizontal plate embedded in a porous medium was studied by Mehta and Rao [8]. Beithou et al. [9] investigated the effects of porosity on free convection flow of non-Newtonian fluids along a vertical plate embedded in a porous medium. Numerical modeling of non-Newtonian fluid flow in a porous medium using a three dimensional periodic array was presented by Inoue and Nakayama [10]. The problem of forced convection heat transfer on a flat plate embedded in porous media for power-law fluids has been studied by Hady and Ibrahim [11]. Katagiri and pop [12] discussed the unsteady laminar free convection near an isothermal horizontal circular cylinder. Also, Aldoss and Ali [13] investigated the problem of mixed convection from a horizontal cylinder in a porous medium. Mohammadien and El-Amin [14] presented the problem of thermal radiation effects on power-law fluids over a horizontal plate embedded in a porous medium. The problem of unsteady and steady-state concentration boundary layer adjacent to a ceiling wall of a stagnation-point flow region resulting from hydrogen impinging leakage is investigated [15-17]. The purpose of this paper is to study the problem of thermal dispersion effects on unsteady free convection from a horizontal circular cylinder to a non-Newtonian fluid saturated porous medium. The Darcy-Brinkman-Forchheimer model which includes the effects of boundary and inertia forces is employed. The dimensionless non-linear partial differential equations are solved numerically using an explicit finite-difference scheme. The values of friction factor and heat transfer coefficient are determined for steady and unsteady free convection.

## 2. Analysis

A schematic diagram of the physical model is shown in Figure 1. Consider the unsteady, laminar boundary layer in a two-dimensional free convective flow of a non-Newtonian fluid over an isothermal horizontal circular cylinder embedded in a porous medium domain. At time $\bar{t} = 0$, the temperature of the surface immersed in the fluid is raised suddenly from that of surrounding fluid $\overline{T}_\infty$, up to a higher and constant value $\overline{T}_w$ and kept at this value thereafter. Under the Boussinesq and boundary layer approximations, the governing mass, momentum and energy conservation equations become:

$$\frac{\partial \bar{u}}{\partial \bar{x}} + \frac{\partial \bar{v}}{\partial \bar{y}} = 0 \tag{1}$$

$$\frac{\partial \bar{u}}{\partial \bar{t}} + \bar{u}\frac{\partial \bar{u}}{\partial \bar{x}} + \bar{v}\frac{\partial \bar{u}}{\partial \bar{y}} = g\beta(\overline{T} - \overline{T}_\infty)\sin\frac{\bar{x}}{R} + \frac{k}{\rho}\frac{\partial}{\partial \bar{y}}\left(\left|\frac{\partial \bar{u}}{\partial \bar{y}}\right|^{n-1}\frac{\partial \bar{u}}{\partial \bar{y}}\right) - \frac{k\varepsilon^n}{\rho \mathrm{K}}|\bar{u}|^{n-1}\bar{u} - \frac{F\varepsilon^2}{\mathrm{K}^{1/2}}|\bar{u}|\bar{u} \tag{2}$$

$$\frac{\partial \overline{T}}{\partial \bar{t}} + \bar{u}\frac{\partial \overline{T}}{\partial \bar{x}} + \bar{v}\frac{\partial \overline{T}}{\partial \bar{y}} = \frac{\partial}{\partial \bar{y}}\{(\alpha + \gamma d\bar{u})\frac{\partial \overline{T}}{\partial \bar{y}}\} \tag{3}$$

In the previous equations, $\bar{u}$ and $\bar{v}$ are the velocity components along $\bar{x}$ and $\bar{y}$ axis. The temperature of the surface is $\overline{T}_w$ and far away from the surface this value is invariant and is represented by $\overline{T}$. $\rho, \alpha, \beta, \varepsilon, F, k, K, \gamma, d$ and $g$ are the density, the thermal diffusivity, the volumetric coefficient of thermal expansion, the porosity, the empirical constant, non-Newtonian consistency index, the permeability, the dispersion coefficient whose value is usually less than 0.3, the pore diameter and acceleration due to gravity, respectively.

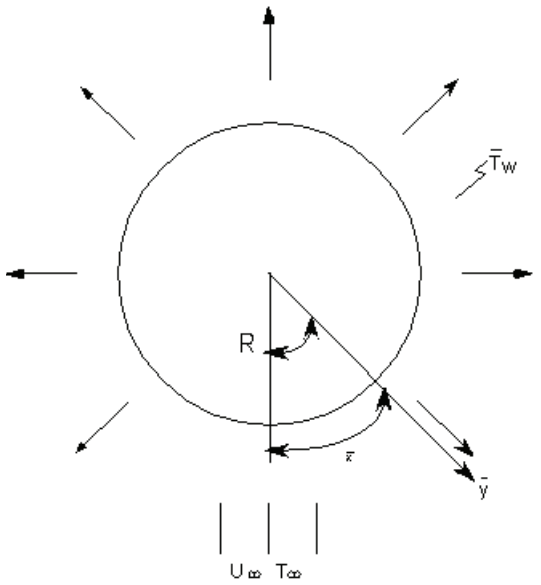


Fig. 1: Flow model and coordinate system

The initial and boundary conditions are:

$$\bar{t}=0:\ \bar{u}=\bar{v}=0,\ \bar{T}=\bar{T}_\infty \quad \text{for all } \bar{x} \text{ and } \bar{y}$$
$$\bar{t}>0:\begin{cases}\bar{u}=\bar{v}=0,\ \bar{T}=\bar{T}_\infty & \text{at } \bar{x}=0\\ \bar{u}=\bar{v}=0,\bar{T}=\bar{T}_w & \text{at } \bar{y}=0,\bar{x}>0\\ \bar{u}=0,\bar{T}=\bar{T}_\infty & \text{at } \bar{y}\to\infty,\bar{x}>0\end{cases} \tag{4}$$

In this study, in accordance with previous work reported by Shulman et al. [18] and Shvets and Vishnevskeiy [19] the following transport properties based on the power-law model are assumed to hold,

$$\tau_{ij}=-p\delta_{ij}+k\left|\frac{1}{2}I_2\right|^{(n-1)/2}e_{ij} \tag{5}$$

where $\tau_{ij}$ and $e_{ij}$ are the tensors of stress and strain rates, $\delta_{ij}$ is the unit tensor, $I_2$ is the second invariant of the strain rate, $p$ is the pressure and $n$ is the power flow behavior index of the fluid ($n$>0). For $n$=1, it reduces to a Newtonian fluid, for values of $n$<1 the behavior is pseudoplastic and, when $n$>1, the fluid is dilatant.

The inertia terms on the left hand side of Equation (2) may be neglected for small permeability. But for higher permeability media, near the leading edge the inertia terms are significant, while the shear stress term remains significant for a large distance.

We introduce the following dimensionless variables,

$$x=\frac{\bar{x}}{R},\ y=\frac{\bar{y}}{R}G^{1/4},\ u=\frac{\bar{u}}{R}G^{1/4},\ v=\frac{\bar{v}}{R}G^{1/2},\ T=\frac{\bar{T}-\bar{T}_\infty}{\bar{T}_w-\bar{T}_\infty}\ \text{and}\ t=\frac{\bar{t}}{G^{1/4}} \tag{6}$$

where $G=[\rho R^2/k]^{4/3}$.

Introducing expressions (6) into Equations (1)-(3) we have the transformed equations in the following form,

$$\frac{\partial u}{\partial x}+\frac{\partial v}{\partial y}=0 \tag{7}$$

$$\frac{\partial u}{\partial t}+u\frac{\partial u}{\partial x}+v\frac{\partial u}{\partial y}=GrT\sin x+\frac{\partial}{\partial y}\left(\left|\frac{\partial u}{\partial y}\right|^{n-1}\frac{\partial u}{\partial y}\right)-k_1|u|^{n-1}u-k_2|u|u \tag{8}$$

$$\frac{\partial T}{\partial t}+u\frac{\partial T}{\partial x}+v\frac{\partial T}{\partial y}=\frac{1}{\Pr}\frac{\partial^2 T}{\partial y^2}+Ds\left[u\frac{\partial^2 T}{\partial y^2}+\frac{\partial u}{\partial y}\frac{\partial T}{\partial y}\right] \tag{9}$$

where $Gr=g\beta(\overline{T}_w-\overline{T}_\infty)G^{1/2}/R$ is the Grashof number, $k_1=\varepsilon^{n}R^{n+1}/KG^{n+1/4}$ and $k_2=F\varepsilon^2R/K^{1/2}$ are the dimensionless first and second-order resistance due to the presence of the solid matrix, $\Pr=R^2/\alpha G^{3/4}$ is the Prandtl number and $Ds=\gamma dG^{1/2}/R$ is the dispersion parameter.

The initial and boundary conditions are now given by,

$$\begin{aligned} &t=0:\ u=v=T=0 && \text{for all } x \text{ and } y\\ &t>0:\begin{cases} u=v=T=0 & \text{at } x=0\\ u=v=0,\ T=1 & \text{at } y=0,\ x>0\\ u=0,\ T=0 & \text{at } y\to\infty,\ x>0 \end{cases} \end{aligned} \tag{10}$$

In technological applications, the wall shear stress and the local Nusselt number are of primary interest.

The wall shear stress may be written as,

$$\tau_w=k\left(\frac{\partial \overline{u}}{\partial \overline{y}}\right)^n\Bigg|_{\overline{y}=0}=k\left(\frac{\partial u}{\partial y}\right)^n\Bigg|_{y=0} \tag{11}$$

Therefore the local friction factor is given by,

$$C_f=\frac{2\tau_w}{\rho R^2}=2G^{-3/4}\left(\frac{\partial u}{\partial y}\right)^n\Bigg|_{y=0} \tag{12}$$

From the definition of the local surface heat flux is defined by,

$$q_w=-(k_e+k_d)\frac{\partial \overline{T}}{\partial \overline{y}}\Bigg|_{\overline{y}=0}=-k_e[1+\Pr\, Ds\, u(x,0)]\frac{\overline{T}_w-\overline{T}_\infty}{R}G^{1/4}\frac{\partial T}{\partial y}\Bigg|_{y=0} \tag{13}$$

where $k_e=\alpha\rho C_p$ is the molecular thermal conductivity, $k_d=\gamma d\overline{u}\rho C_p$ is the dispersion thermal conductivity of the saturated porous medium, together with the definition of the local Nusselt number,

$$Nu=\frac{q_w}{\overline{T}_w-\overline{T}_\infty}\frac{R}{k_e}=-G^{1/4}[1+\Pr\, Ds\, u(x,0)]\frac{\partial T}{\partial y}\Bigg|_{y=0} \tag{14}$$

## 3. Method of Solution

This section is concerned with the numerical method used in the solution of the present unsteady problem. The solution of a set of three, simultaneous, nonlinear partial differential equations by the finite-difference method, employing an explicit technique (a simple example with more details was explained by Carnahan et al. [20]). The numerical integration was carried out on the time dependent form of the nonlinear partial differential Eqs. (7)-(9), subject to the initial and boundary conditions (10).

Successive steps in time may be regarded as successive approximations towards the final steady state solution, for which both $\partial u/\partial t$ and $\partial T/\partial t$ are zeros, one way such a solution may be achieved is by considering the corresponding unsteady state problem. The spatial domain under investigation must be restricted to finite dimensions. We consider $x_{\max}$=50, and regarded $y$=$y_{\max}$=20 as corresponding to $y=\infty$.

An explicit method will be used. Consider $u', v'$ and $T'$ denote the values of u, v and T at the end of a time-step. A selection set of results have been obtained covering the ranges $0.5 \le n \le 2.0$, $0.0 \le Ds \le 0.5$, $5 \le \Pr \le 10$, $1 \le Gr \le 3$, $0.03 \le k_1 \le 0.05$ and $0.02 \le k_2 \le 0.04$. The steady state condition was assumed to exist when $\partial u/\partial t$, and $\partial T/\partial t$ approached zero in the unsteady state problem. The system of equations were solved for the dependent variables $u$, $v$ and $T$ as functions of $x$, $y$ and $t$. Successive steps in time can then be regarded as successive approximations toward the steady state solution. The velocity and temperature fields were calculated for various time steps for a 25×10 grid. An examination of complete results for $t$=10, 20,..., 90, revealed little or no change in $u$, $v$ and $T$ after $t$=90 for all computations. Thus the results for $t$=90 are essentially the steady-state values.

## 4. Stability Conditions

Here, the stability conditions of the finite difference scheme are determined. Because an explicit scheme has been used, we investigate the consistency of the largest time-step with the numerical stability. At an arbitrary time $t$=0, the general terms of the Fourier expansion for $u$ and $T$ are $e^{i(ax+by)}$, $i=\sqrt{-1}$. At a later time t, these terms become $u=\psi(t)e^{i(ax+by)}$, $T=\zeta(t)e^{i(ax+by)}$.

Substituting in the corresponding difference equations and regarding the coefficients $u$ and $v$ as constants over any one time-step and denoting the values of $\psi$ and $\zeta$ after the time-step by $\psi'$ and $\zeta'$, we obtain,

$$\frac{\psi'-\psi}{\Delta t}+u\frac{\psi(1-e^{-ia\Delta x})}{\Delta x}+v\frac{\psi(e^{ib\Delta y}-1)}{\Delta y}=Gr\sin(i\Delta x)\zeta'+\psi\left\{\left|\frac{u_{i,j+1}-u_{i,j}}{\Delta y}\right|^{n-1}\left(\frac{(e^{ib\Delta y}-1)}{\Delta y}\right)-\left|\frac{u_{i,j}-u_{i,j-1}}{\Delta y}\right|^{n-1}\left(\frac{(1-e^{-ib\Delta y})}{\Delta y}\right)\right\}\Big/\Delta y-k_1|u|^{n-1}\psi-k_2|u|\psi \tag{15}$$

$$\frac{\zeta'-\zeta}{\Delta t}+u\frac{\zeta(1-e^{-ia\Delta x})}{\Delta x}+v\frac{\zeta(e^{ib\Delta y}-1)}{\Delta y}=2\zeta\left(\frac{1}{\Pr}+Ds\,u\right)\frac{(\cos b\Delta y-1)}{(\Delta y)^2}+Ds\,\zeta\left(\frac{u_{i,j+1}-u_{i,j}}{\Delta y}\right)\left(\frac{(e^{ib\Delta y}-1)}{\Delta y}\right) \tag{16}$$

We note that the coefficients $\left|(u_{i,j+1}-u_{i,j})/\Delta y\right|^{n-1}$ and $\left|(u_{i,j}-u_{i,j-1})/\Delta y\right|^{n-1}$ are very close to unity, because, the choice the exponent lie in the interval $-0.5 \le n-1 \le 1$. We assume that,

$$A = 1 - \frac{u\Delta t}{\Delta x}(1 - e^{-ia\Delta x}) - \frac{v\Delta t}{\Delta y}(e^{ib\Delta y} - 1) + \frac{\Delta t}{(\Delta y)^2}\left\{\left|\frac{u_{i,j+1} - u_{i,j}}{\Delta y}\right|^{n-1}(e^{ib\Delta y} - 1) - \left|\frac{u_{i,j} - u_{i,j-1}}{\Delta y}\right|^{n-1}(1 - e^{-ib\Delta y})\right\} - k_1|u|^{n-1} - k_2|u| \tag{17}$$

$$B = 1 - \frac{u\Delta t}{\Delta x}(1 - e^{-ia\Delta x}) - \frac{v\Delta t}{\Delta y}(e^{ib\Delta y} - 1) + \frac{2\Delta t(1 + \Pr Ds\, u)}{\Pr(\Delta y)^2}(\cos b\Delta y - 1) + \frac{Ds\Delta t}{(\Delta y)^2}(u_{i,j+1} - u_{i,j})(e^{ib\Delta y} - 1) \tag{18}$$

Using Equations (15)-(18), one can write,

$$\psi' = A\psi + \Delta t Gr \sin(i\Delta x)\zeta' = A\psi + \Delta t Gr \sin(i\Delta x)B\zeta$$
$$\zeta' = B\zeta$$

or

$$\begin{bmatrix}\psi' \\ \zeta'\end{bmatrix} = \begin{bmatrix}A & GrB\Delta t \sin(i\Delta x) \\ 0 & B\end{bmatrix}\begin{bmatrix}\psi \\ \zeta\end{bmatrix}$$

In order to seek the stability of the previous system, the moduli of each of the eigen values $\lambda_1$ and $\lambda_2$ of the coefficients matrix should be less than or equal to unity. Here, we have $\lambda_1 = A$ and $\lambda_2 = B$. Therefore, the stability conditions are $|A| \le 1$ and $|B| \le 1$, for all *a* and *b*.

Since, the heated fluid rises in the positive *x*-direction, *u* may be assumed everywhere non-negative. Also, we assume that *v* to be everywhere non-positive, because, the fluid is drawn in from the positive *y*-direction to take its place. We can assume, at any case, that,

$$\alpha = \frac{u\Delta t}{\Delta x},\ \beta = \frac{|v|\Delta t}{\Delta y},\ \gamma = \frac{\Delta t}{(\Delta y)^2},\ \delta = \frac{u\Delta t}{(\Delta y)^2},\ c_1 = \left|(u_{i,j+1} - u_{i,j})/\Delta y\right|^{n-1},$$
$$c_2 = \left|(u_{i,j} - u_{i,j-1})/\Delta y\right|^{n-1},\ c_3 = k_1|u|^{n-1},\ c_4 = k_2|u| \text{ and } c_5 = |u_{i,j+1} - u_{i,j}|$$

Therefore,

$$A = 1 - \alpha(1 - e^{-ia\Delta x}) - \beta(e^{ib\Delta y} - 1) + \gamma\left\{c_1(e^{ib\Delta y} - 1) - c_2(1 - e^{-ib\Delta y})\right\} - c_3 - c_4$$
$$B = 1 - \alpha(1 - e^{-ia\Delta x}) - \beta(e^{ib\Delta y} - 1) + 2(\frac{\gamma}{\Pr} + Ds\delta)(\cos b\Delta y - 1) + Dsc_5\gamma(e^{ib\Delta y} - 1)$$

The coefficients $\alpha, \beta, \gamma$ and $\delta$ are positive and real. Representing *A* and *B* on an Argand diagram, the maximum values of $|A|$ and $|B|$ occur when $a\Delta x = r\pi$ and $b\Delta y = s\pi$, where r and s are positive integers. The values of $|A|$ and $|B|$ are maximum, for $\Delta t$ sufficiently large, when both r and s are odd integers. In this case we have,

$$A = [1 - \alpha - \beta - \gamma(c_1 + c_2)] - \alpha - \beta - \gamma(c_1 + c_2) - c_3 - c_4$$
$$= 1 - 2[\alpha + \beta + \gamma(c_1 + c_2)] - c_3 - c_4$$

$$B = [1-\alpha-\beta-2(\frac{\gamma}{\Pr}+Ds\delta)-Dsc_3\gamma]-\alpha-\beta-2(\frac{\gamma}{\Pr}+Ds\delta)-Dsc_5\gamma$$

$$= 1-2[\alpha+\beta+2(\frac{\gamma}{\Pr}+Ds\delta)+Dsc_3\gamma]$$

To satisfy $|A| \le 1$ and $|B| \le 1$ the most negative allowable value is $A$=$B$=-1, then, the stability conditions can be written as,

$$-1 \le 1-2[\alpha+\beta+\gamma(c_1+c_2)]-c_3-c_4$$

$$-1 \le 1-2[\alpha+\beta+2(\frac{\gamma}{\Pr}+Ds\delta)+Dsc_3\gamma]$$

or

$$\alpha+\beta+\gamma(c_1+c_2)+\frac{c_3+c_4}{2} \le 1 \quad (19)$$

$$\alpha+\beta+2(\frac{\gamma}{\Pr}+Ds\delta)+Dsc_3\gamma \le 1 \quad (20)$$

In order to aid the first stability condition (19) to satisfy, we choice $0.03 \le k_1 \le 0.05$ and $0.02 \le k_2 \le 0.04$, which make values of $c_3$ and $c_4$ more small, with noting that $c_1$ and $c_2$ close to unity as explained above. Also, the choice $0.0 \le Ds \le 0.5$ and $5 \le \Pr \le 10$ aid the second stability condition (20) to satisfy.

## 5. Results and Discussion

Equations (7)-(9) subject to the conditions equation (10) were solved by the finite difference method. Figures 2-5 illustrate the velocity profiles for different values of the parameters $t$, $n$, $Ds$, $k_1$, $k_2$, Pr and $Gr$. Figure 2 illustrates the development of the velocity field with time until steady-state conditions are achieved with various values of $n$. As time increases, we observe that the momentum boundary layer thickens and the velocity maximum increases. Also, from the same figure we note that as the power-law index $n$ increases the velocity maximum increases near the surface, while it decreases far from the surface. Figure 3 indicates that as the dispersion parameter $Ds$ increases the velocity maximum increases. We observe from Figure 4 that as the parameters $k_1$ and $k_2$ increase, the velocity maximum decreases. Figure 5 display results for velocity profiles with various values of the parameters Pr and $Gr$.

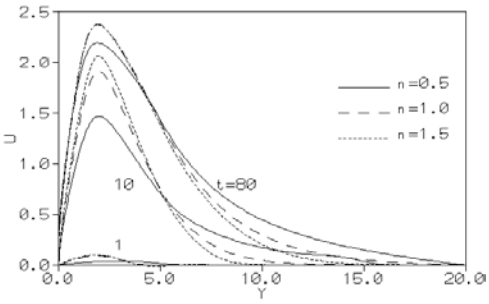


Fig. 2. Transient velocity profiles for various values of $n$ when $k_1$=0.04, $k_2$=0.04, $Ds$=0.05, $Gr$=3.0 and $Pr$=5.0 at $X$=20.

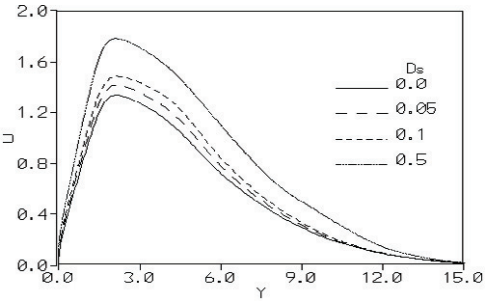


Fig. 3. Steady state velocity profiles for various values of $Ds$ when $n$=1.5, $k_1$=0.03, $k_2$=0.04, $Gr$=1.0 and Pr=5.0 at $X$=20.

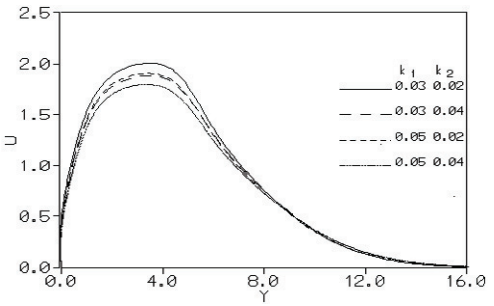


Fig. 4. Steady state velocity profiles for various values of $k_1$ and $k_2$ when $n$=1.5, $Gr$=1.0, Ds=5.0 and Pr=5.0 at $X$=20.

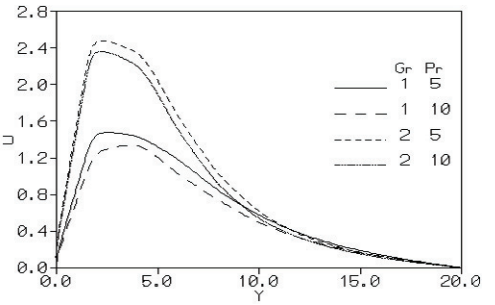


Fig. 5. Steady state velocity profiles for various values of Pr and $Gr$ when $n$=0.5, $k_1$=0.05, $k_2$=0.04, $Ds$=0.5 at $X$=20.

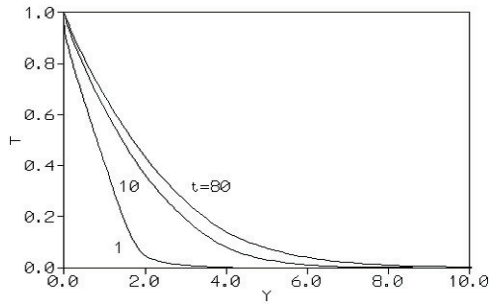


Fig. 6. Transient temperature profiles when $n$=0.5, $k_1$=0.04, $k_2$=0.04, $Ds$=0.05, $Gr$=3.0 and $Pr$=5.0 at $X$=20.

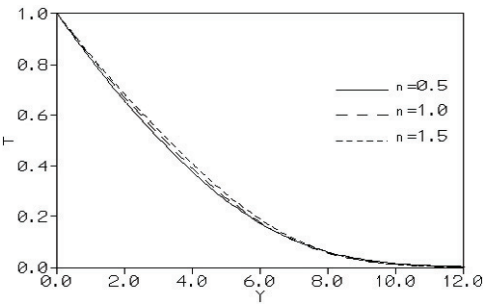


Fig. 7. Steady state temperature profiles for various values of $n$ when $Ds$=0.5, $k_1$=0.05, $k_2$=0.04, $Gr$=2.0 and Pr=10.0 at $X$=20.

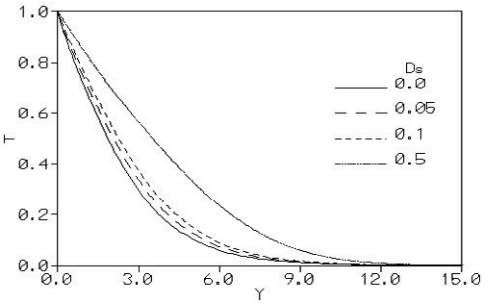


Fig. 8. Steady state temperature profiles for various values of $Ds$ when $n$=1.5, $k_1$=0.03, $k_2$=0.04, $Gr$=1.0 and Pr=5.0 at $X$=20.

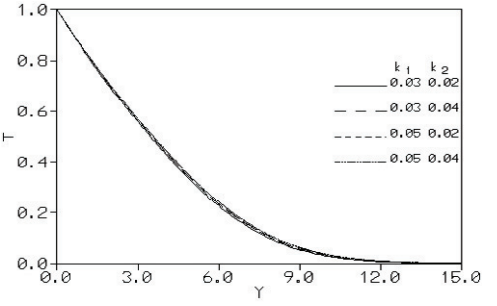


Fig. 9. Steady state temperature profiles for various values of $k_1$ and $k_2$ when $n$=1.5, $Gr$=1.0, $Ds$=0.5 and Pr=5.0 at $X$=20.

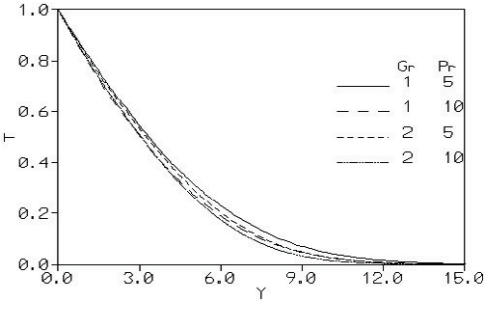


Fig. 10. Steady state temperature profiles for various values of Pr and $Gr$ when $n$=0.5, $k_1$=0.05, $k_2$=0.04 and $Ds$=0.5 at $X$=20.

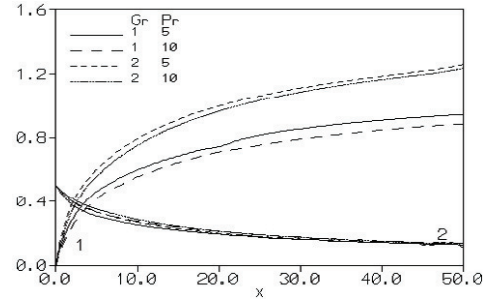


Fig. 11. Steady state 1: friction factor and 2: Nusselt number against $X$ for various values of $Gr$ and Pr at $n$=0.5, $k_1$=0.05, $k_2$=0.04 and $Ds$=0.5.

Table 1. Transient friction factor and Nusselt number for various values of $t$ and $n$ with $Ds$=0.05, $Gr$=3 and $Pr$=5, and $k_1$= $k_2$=0.04 at $X$=20.

| $t$ | $n$ | $(G^{3/4}/2)C_f$ | Nu |
|---|---|---|---|
| 20 | 0.5 | 1.048574 | 0.282863 |
| | 1.0 | 1.186271 | 0.285182 |
| | 1.5 | 1.287733 | 0.282085 |
| 40 | 0.5 | 1.047163 | 0.284135 |
| | 1.0 | 1.187660 | 0.286065 |
| | 1.5 | 1.290524 | 0.282775 |
| 60 | 0.5 | 1.047169 | 0.284131 |
| | 1.0 | 1.187685 | 0.286085 |
| | 1.5 | 1.290595 | 0.282799 |
| 90 | 0.5 | 1.047172 | 0.284134 |
| | 1.0 | 1.187687 | 0.286086 |
| | 1.5 | 1.290603 | 0.282802 |
| $\infty$ | 0.5 | 1.047172 | 0.284134 |
| | 1.0 | 1.187687 | 0.286086 |
| | 1.5 | 1.290603 | 0.282802 |

Table 2. Steady state friction factor and Nusselt number for various values of $k_1$, $k_2$ and $Ds$ when $Gr$=1, Pr=5 and $n$=1.5 at $X$=20.

| $k_1$ | $k_2$ | $Ds$ | $(G^{3/4}/2)C_f$ | $Nu/G^{1/4}$ |
|---|---|---|---|---|
| 0.03 | 0.02 | 0.0 | 0.581699 | 0.269590 |
| | | 0.05 | 0.636521 | 0.248320 |
| | | 0.1 | 0.685050 | 0.230333 |
| | | 0.5 | 0.916303 | 0.154709 |
| | 0.04 | 0.0 | 0.546717 | 0.264694 |
| | | 0.05 | 0.595453 | 0.243836 |
| | | 0.1 | 0.638364 | 0.226196 |
| | | 0.5 | 0.838565 | 0.151977 |
| 0.05 | 0.02 | 0.0 | 0.549908 | 0.265083 |
| | | 0.05 | 0.600150 | 0.244294 |
| | | 0.1 | 0.644621 | 0.226686 |
| | | 0.5 | 0.855543 | 0.152423 |
| | 0.04 | 0.0 | 0.519354 | 0.260582 |
| | | 0.05 | 0.564318 | 0.240174 |
| | | 0.1 | 0.603918 | 0.222889 |
| | | 0.5 | 0.788280 | 0.149886 |

We note that as $Pr$ increases the maximum velocity decreases, while it increases as $Gr$ increases. Figures 6-10 show the temperature profiles for different values of the given parameters. Figure 6 illustrate the development of the temperature field with time. The thermal boundary layer thickness increases with time. We note that as the power-

law index $n$ increases the temperature profiles increase, as plotted in Figure 7. It is clear from Figure 8 that as the dispersion parameter $D_s$ increases the temperature profiles increase. Also, Figure 9 indicates that both $k_1$ and $k_2$ enhances the temperature profiles. Furthermore, we observe from Figure 10 that due to an increase in the parameters $Pr$ and $Gr$ there is a fall in the temperature profiles. In Figure 11, friction factor and Nusselt number are plotted as functions of $X$ for various values of the parameters $Pr$ and $Gr$. It is clear from this figure that $Gr$ enhances the wall shear stress and the heat transfer rate but they are reduced as $Pr$ increases.

Table 1 represents the variation of friction factor and Nusselt number for pseudoplastic fluid ($n$<1), Newtonian fluid ($n$=1) and dilatant fluid ($n$>1) with various values of the time. From Table 2 it can be seen that due to an increase in $Ds$ there is an increase in the wall shear stress and a fall in the heat transfer rate. Also, from the same table we note that both the parameters $k_1$ and $k_2$ reduces the wall shear stress and the heat transfer rate.

## References

[1] P. Cheng, Thermal dispersion effects in non-Darcian convective flows in a saturated porous medium, Lett. Heat Mass Transfer 8 (1981) 267.

[2] O. A. Plumb, The effect of thermal dispersion on heat transfer in packed bed boundary layers, Proc. of 1st ASME/JSME Thermal Engineering Joint Conf. 2 (1983) 17.

[3] M. A. Mansour and M. F. El-Amin, Thermal dispersion effects on non-Darcy axisymmetric free convection in a saturated porous medium with lateral mass transfer, Appl. Mech. Eng. 4 (1999) 727.

[4] A. A. Mohammadein and M. F. El-Amin, Thermal dispersion–radiation effects on non-Darcy natural convection in a fluid saturated porous medium, Transport in Porous Media, 40 (2000) 153.

[5] H.T. Chen and C.K. Chen, Natural convection of non-Newtonian fluids along a vertical plate embedded in a porous medium, Trans. ASME, J. Heat Transfer 110 (1998) 257.

[6] A. Nakayama and H. Koyama, Buoyancy induced flow of non-Newtonian fluids over a non-isothermal body of arbitrary shape in a fluid-saturated porous medium, Applied Scientific Research 48 (1991) 55.

[7] A.V. Shenoy, Darcy-Forchheimer natural, forced and mixed convection heat transfer in non-Newtonian power-law fluidsaturated porous media, Trans. in Porous Media 11 (1993) 219.

[8] K.N. Mehta and K.N. Rao, Buoyancy-induced flow of non-Newtonian fluids over a non-isothermal horizontal plate embedded in a porous medium , Int. J. Eng. Sc. 32 (1994) 521.

[9] N. Beithou, K., Albayrak, and A. Abdulmajeed, Effects of porosity on the free convection flow of non-Newtonian fluids along a vertical plate embedded in a porous medium, Turkish J. of Eng. Envir. Sci., 22 (1999) 203.

[10] M. Inoue and A. Nakayama, Numerical modeling of non-Newtonian fluid flow in a porous medium using a three dimensional periodic array, Trans. ASME, J. of Fluid Eng., 120 (1998) 131.

[11] F.M. Hady and F.S. Ibrahim, Forced convection heat transfer on a flat plate embedded in porous media for power-law fluids , Trans. in porous media, 28 (1997) 125.

[12] M. Katagiri and I. Pop, Transient free convection from an isothermal horizontal circular cylinder, Warme und Stoffubertragung 12 (1979) 73.

[13] T. K. Aldoss and Y. D. Ali, MHD mixed convection from a horizontal cylinder in a porous medium, JSME Int. J., Series B 40 (1997) 290.

[14] A. A. Mohammadien and M. F. El-Amin, Thermal radiation effects on power-law fluids over a horizontal plate embedded in a porous medium, Int. commun. heat mass transfer 27 (2000) 1025.

[15] M. F. El-Amin and H. Kanayama, Boundary layer theory approach to the concentration layer adjacent to a ceiling wall at impinging region of a hydrogen leakage, Int. J. Hydrogen Energy 33 (2008) 6393.

[16] M. F. El-Amin, M Inoue and H. Kanayama, Boundary layer theory approach to the concentration layer adjacent to the ceiling wall of a hydrogen leakage: Far region, Int. J. Hydrogen Energy 33 (2008) 7642.

[17] M. F. El-Amin and H. Kanayama, Boundary layer theory approach to the concentration layer adjacent to the ceiling wall of a hydrogen leakage: Axisymmetric impinging and far regions, Int. J. Hydrogen Energy 34 (2009) 1620.

[18] Z. P. Shulman, B. I. Baykov and E. A. Zaltsgendler, Heat and mass transfer in free convection of non-Newtonian fluids, Naukai technika, Minsk (1975), in Russian.

[19] Yu. I. Shvets and V.K. Vishevskiy, Effect of dissipation on convective heat transfer in flow of non-Newtonian fluids, Heat Transfer-Soviet Research 19 (1987) 38.

[20] B. Carnahan, H.A. Luther J.O. Wilkes, Applied numerical methods, John Wiley, New York, 1969.